Neutrinos for non-proliferation

Mitigation of backgrounds from photomultiplier radioactivity for reactor antineutrino monitoring

Elisabeth Kneale, University of Sheffield

October 24, 2018

Abstract

Identifying the existence of a clandestine reactor in a complex nuclear landscape for nuclear threat reduction is challenging. WATCHMAN will demonstrate for the first time the feasibility of detecting the signal from a hidden reactor against the background of a second reactor.

A kilotonne-scale detector to be built underground in the Boulby Mine in North Yorkshire, WATCHMAN will detect antineutrinos - the unshieldable by-product of radioactive decay in a nuclear reactor.

A WATCHMAN-style detector could be used remotely as part of a non-proliferation agreement and WATCHMAN offers a unique opportunity to develop reactor antineutrino detection technology for non-proliferation and beyond.

Such a detector will out of necessity operate at long range, often at the very limit of its sensitivity, and so minimising backgrounds is essential. Photomultipliers (PMTs) detect light from antineutrino interactions in the detector however accidental coincidences from the decay of radioactive isotopes in PMT glass mimic the antineutrino signal and are one of the principle sources of backgrounds for the experiment.

This paper presents an analytical method for optimising the signal-to-background ratio in the experimental results and uses it to compare the relative benefits of different PMT types. It is found that while the optimal detector design uses 10" low radioactivity glass PMTs, the potentially stronger and more readily available 12" standard-glass PMTs can give comparable results due to the improvement in the precision with which we can identify exactly where in the detector an event has occurred. This result is sensitively dependent on the dark noise rate in the tubes due to its effect on reconstruction at lower energies.

1 Introduction

In 2011, the National Nuclear Security Administration (NNSA) in the USA published its Strategic Plan [1], which called for the demonstration of remote reactor monitoring for nuclear non-proliferation.

The challenge of remote reactor monitoring is to not only detect the existence of a reactor, but also to differentiate its signal from other reactor backgrounds by a combination of location and core composition information. The ability to determine when a quantity of material - namely weapons-grade plutonium - is removed is also key for non-proliferation.

In a nuclear reactor, energy is produced by the fission of $^{235}U, ^{238}U, ^{239}Pu$ and ^{241}Pu into neutron-rich nuclei, which then undergo a series of β decays to stability. The beta decay reaction $(n \longrightarrow p + e^- + \overline{\nu}_e)$ produces on average ~ 6 electron antineutrinos $(\overline{\nu}_e)$ per fission. The resulting antineutrino flux is $1.5 \times 10^{20} \text{s}^{-1}$ from a 1GW reactor [?] so that, although the interaction cross section (probability of an interaction) of antineutrinos with matter is very small at $\mathcal{O}(10^{-43} \text{ cm}^2)$, an enormous number of antineutrinos is released and these can be seen in a variety of types of detectors such as Double Chooz [2], PROSPECT [3] and DANSS [4].

The antineutrino flux and energy spectrum bear the imprints of the core power, composition and location [5] [6] [7]. So antineutrino detection can potentially meet the requirements of remote monitoring for non-proliferation, particularly when used in conjunction with other monitoring methods e.g. satellite imaging.

The WATCHMAN WATer CHerenkov Monitor for ANtineutrinos (section 3.1) will be a prototype gadolinium-doped (section 2.2) water Cherenkov detector (section 2.1) for detecting reactor antineutrinos and will be built in the UK. Like a detector for use in the field, it will operate at the very limit of its sensitivity and it is therefore essential to minimise backgrounds in the detector through both practical and analytical methods.

Photomultiplier tubes (PMTs) are used to detect light from reactor antineutrino interactions in the detector. They are also a priciple source of backgrounds to the signal. This paper presents the use of an analytical method of signal-to-background optimisation to compare three different types of PMT in order to maximise detector sensitivity within the constraints of the project.

2 Reactor antineutrino detection

2.1 Water Cherenkov detectors for antineutrinos

Water Cherenkov detectors are essentially tanks of water instrumented with PMTs, which detect 'Cherenkov' light produced as a result of neutrino interactions in water.

Antineutrinos from a reactor interact with protons (hydrogen nuclei) in the water via the inverse β decay (IBD) interaction $\overline{\nu}_e + p \longrightarrow n + e^+$ and emit a positron (e^+) and a neutron (n).

Charged particles from these interactions can travel faster than the local speed of light in water ($v > c/n_r$, where $n_r = 1.33$ is the refractive index of water) and emit a cone of blue radiation, or Cherenkov cone, which can be detected via the PMTs on the walls of the detector as a Cherenkov ring or ellipse, depending on the angle of approach.

In a PMT, Cherenkov photons hit a photocathode on the front of a glass vacuum tube and are converted to photoelectrons. These photoelectrons are then accelerated along a chain of dynodes, each of which multiply the number of electrons by a characteristic factor. The multiplied signal is then read out at the anode at the back of the PMT.

The energy of the charged particle and interaction vertex (position of the IBD interaction in the detector) can be reconstructed from a Cherenkov ring pattern which is distributed over a minimum of 4 PMTs [8]. The velocity of the particle can be calculated from the Cherenkov angle (the angle the Cherenkov cone makes with the direction of the charged particle). For low-energy reactor antineutrinos, the energy of the positron is found using the velocity to calculate the distance to the interaction vertex and the intensity of the light detected in terms of the number of hits on the PMTs. The energy of the incident antineutrino is then simply related to the energy of the positron [9].

2.2 Gd-H_2O for low-energy reactor antineutrinos

The peak energy of a reactor antineutrino is very close to the detection limit of a water Cherenkov detector. The solution is to dissolve a low concentration of gadolinium (Gd) in the detector water.

The principle of using Gd to extend into lower-energy neutrino detection was first introduced by [10] and developed by [11]. Without Gd, the neutron from the IBD reaction in the detector thermalises in the water and captures onto a hydrogen nucleus. With Gd in the water, the neutron captures preferentially onto the Gd nucleus. This creates Gd in an excited state, which then undergoes γ decay to its stable state, emitting a relatively high-energy γ cascade of $\sim 8\mathrm{MeV}$ (mean total energy). These γ rays scatter off electrons in the water, which can then emit Cherenkov light if they gain sufficient energy. This gives a correlated signal from the IBD reaction [11], with the Cherenkov light from the positron and subsequent neutron capture occurring within $\sim 30\mu\mathrm{s}$ and $\sim 50\mathrm{cm}$.

The correlated signal consists of a prompt emission of Cherenkov radiation with a peak at $\sim 2.5\mathrm{MeV}$ and a delayed neutron-capture emission with a peak at $\sim 4\mathrm{MeV}$. Since the mean energy of the positron emission is at the limit of the detection threshold for water Cherenkov detectors, Gd makes it possible to first detect the neutron and then work backwards to find the correlated prompt signal. Thus Gd significantly increases the sensitivity of a water Cherenkov detector to low-energy reactor antineutrinos.

The optimal concentration of Gd in water has been found to be 0.1% Gd ions. At this concentration, over 80% and up to more than 90% [11] of the neutrons capture onto Gd. The remaining neutrons capture onto the hydrogen in the water. Beyond this concentration, the Gd

begins to crystallise out of solution.

The EGADS (Evaluating Gadolinium's Actions on Detector Systems) molecular band-pass filter water-purification system [12] has proven that gadolinium sulphate-doped water can be purified to ∼100m attenuation lengths to over 90% of Super-K ultra-pure levels during stable operation.

3 Antineutrino detectors for nuclear non-proliferation

The Advanced Instrumentation Testbed (AIT) is a US-UK collaboration, with primary funding under the 2011 Strategic Plan in the USA and by the Ministry of Defence. The ultimate goal of AIT is to create kilotonne- to megatonne-scale detectors to detect, locate or exclude the existence of undeclared 50MW-scale fission reactors between tens and hundreds of km away.

3.1 WATer Cherenkov Monitor for ANtineutrinos (WATCHMAN)

WATCHMAN is the first phase of AIT and its aim is to demonstrate the ability to detect the duty cycle of a reactor against the background of a second reactor within a 25km radius.

The WATCHMAN detector will be a ∼6-kilotonne water Cherenkov detector doped with 0.2% concentration by weight of gadolinium sulphate ($Gd_2(SO_4)_3$).

Its baseline design (figure 1) is a cylinder 20m in diameter and height with a 1-kilotonne 'fiducial volume'. The fiducial volume is a 'virtual' volume, defined in the analysis, from which events are selected. Events occuring outside the fiducial volume are cut from the analysis for the purpose of background reduction.

The tank will be instrumented with around 4400 low radioactive intensity (LRI) $10''$ PMTs facing in towards the fiducial volume and around 440 PMTs facing outwards to create a 'veto' volume between the tank wall and PMT support structure. The purpose of the veto volume is to eliminate backgrounds from cosmic ray muons and tank/cavern radioactivity.

This number of inner PMTs corresponds to 25% coverage of the surface area of the inner volume. Beyond 25%, the increase in sensitivity with coverage falls off, due in part to the increase in backgrounds from PMT glass radioactivity.

The final internal detector design has not yet been finalised and studies are underway to determine the optimal design as a function of both sensitivity and cost.

The detector will be located in a 25m cylindrical cavern 1km underground in ICL UK's Boulby Mine near Whitby in North Yorkshire. The advantages of the Boulby Mine location are the low backgrounds, the existing Science & Technology Funding Council (STFC) Boulby Underground Laboratory and its location 25km from the Hartlepool 3GW reactor. The Hartlepool reactor is a twin-core reactor and so is ideally suited to the WATCHMAN goal of demonstrating the ability to detect a reactor against the background of a second reactor.
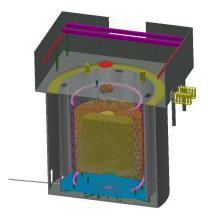
Figure 1: WATCHMAN baseline conceptual design by JG Bossevain Design

3.1.1 Advanced Instrumentation Testbed (AIT) phases 2 & 3

After WATCHMAN Phase One, the detector will become a testbed for advanced technologies such as water-based liquid scintillator (WbLS) and advanced photosensors.

WbLS [13] is achieved by the addition of micelles with one hydrophilic end and one hydrophobic end. These enable the combination of the oil-like liquid scintillator with water. The concentration of liquid scintillator can be tuned to the specific needs of the detector. The advantage of using WbLS is the combination of scintillation and Cherenkov light. This enables detection of lower-energy antineutrinos and, when used in conjunction with picosecond photodetectors, determination of the direction of travel of the antineutrinos to give separation of the prompt Cherenkov light and later scintillation light.

Examples of advanced photosensors are large-area picosecond photodetectors (LAPPDs) [14] and multiple photomultiplier tubes (mPMTs) [15].

The picosecond timing resolution and millimetre spatial resolution of LAPPDs combined with WbLS would enable separation of the prompt Cherenkov and delayed scintillator signals, making it possible to achieve not only improved sensitivity but also directionality. Although mPMTs have tens of picosecond timing rather than picosecond timing, the benefit of mPMTs is their lower cost compared to LAPPDs and improved timing and reconstruction compared to single PMTs.

The ultimate goal of AIT is to develop a megatonne-scale water Cherenkov detector which can be used in the field to detect an unkown reactor up to $\sim 1000 \mathrm{km}$ away.

4   Backgrounds in WATCHMAN

The time- and distance-correlated signal of the IBD and subsequent neutron capture on gadolinium allows many of the backgrounds to be minimised or removed. However there are sources of both correlated and uncorrelated backgrounds which can mimic the correlated antineutrino signal.

Correlated backgrounds are due to the influx of cosmic ray muons to the detector and in the rock surrounding the cavern. Accidental coincidences of two physically independent (uncorrelated) interactions are due to natural radioactivity in the detector materials.

The rate of accidental coincidences depends on the composition of the detector (PMTs, water, $Gd_2(SO_4)_3$, steel, concrete and surrounding rock), the energy threshold and vertex position, vertex resolution, and the distance of the fiducial volume from the detector and cavern materials. The relevant decays/parts of the decay chains are of isotopes with a non-negligible half-life and energy around or above the Cherenkov threshold.

^{238}U, ^{232}Th and ^{40}K are sources of radioactivity in the PMT glass. The ^{238}U and ^{232}Th decay chains in particular contribute significant backgrounds and the PMTs will be the principal source of accidental coincidences in WATCHMAN.

5   PMT optimisation

Optimisation of the PMTs is a combination of maximising detection and reconstruction efficiencies while reducing backgrounds due to PMT contamination with radioactive isotopes. This can be achieved through both practical and analytical methods: using Low Radioactive Intensity (LRI) PMTs, using a PMT with a larger area and better timing characteristics and using analytical methods to select only those events above a minimum energy and distance from the PMT.

A limit on the supply rate and concerns over the strength of LRI glass have motivated feasibility studies looking at whether it is possible to achieve comparable sensitivity with standard glass (SG) PMTs. For this reason, the comparison between LRI and the less expensive SG is vital in establishing the optimal sensitivity that can be achieved within the financial and logistical constraints of the project.

Another method is to define a 'buffer' volume between the inward-facing PMTs and the fiducial volume. Since the rate of radioactive decay from PMTs falls off exponentially with distance from the PMT, cutting from the analysis events within this buffer volume cuts out a large proportion of backgrounds due to PMT radioactivity.

The investigation has centered on the LRI R7801 10", the SG R7801 10" and the SG R11780 12" Hamamatsu PMTs.

5.1 PMT characteristics

The radioactivity rates for ^{238}U, ^{232}Th and ^{40}K are up to ten times higher in standard glass (table 1) and so backgrounds in the detector from standard glass are substantially higher.

Isotope	R7801 HQE (ppm)	R11780 HQE (ppm
238U	0.04	0.341
232Th	0.13	1.33
40K	36	260

Table 1: Radioactivity rates for LRI and SG PMTs (samples counted for Hamamatsu PMTs in 2014).

PMT characteristics which affect detection and reconstruction efficiencies can contribute to background suppression.

The 12" PMT has a spherical shape compared to the 10" PMT. This results in a larger effective area for the same end-on PMT coverage. With an effective area of 1.62 times the area of the 10" PMT, the area of the 12" PMT is proportionately higher by a factor of 1.125 [16], which could increase the detection efficiency for the same PMT coverage. Conversely, this means that the mass of glass is proportionately higher in the 12" PMT, therefore radioactivity levels will also be proportionately higher.

The shape of the PMT's anode output signal affects a PMT's timing and resolution [17]. The transit time distribution for a single photoelectron (SPE) response is used to characterise this signal. Transit time is the time from the absorption of a photoelectron and creation of a photon at the photocathode at the PMT face to the output of the resulting signal at the anode at the back of the PMT. The SPE transit time distribution has a number of features as discussed in [18]. Most notably, there is an initial Gaussian signal peak, a late pulsing peak (caused by scattering and reflection within the PMT) and a continuous but random distribution of dark noise events (caused by thermal electron emission from the PMT photocathode). The transit time spread or jitter of the PMT is the standard deviation of the promt signal peak [18]. The size of the jitter has a significant impact on our ability to reconstruct the vertex.

Table 2 shows the timing characteristics of the 10" PMT and the 12" PMT. The transit time spread in terms of the standard deviation of the prompt signal of the 12" PMT is 1.29ns compared to 1.44ns for the 10" PMT [18] [19]. The high late pulsing fraction of the 12" PMT is thought to be in part due to multiple photons which have not been corrected for [18]. The timing characteristics of the 12" PMT are excellent in comparison to the 10" PMT.

	R7801 HQE (1500V)	R11780 HQE (1900V)
Transit time spread σ_{prompt} (ns)	1.44	1.29
Transit time spread FWHM (ns)	3.40	3.03
Dark noise (Hz)	8000.00	4428.00
Late pulsing (%)	4.00	4.48

Table 2: Timing characteristics of the R7801 and R11780, operating voltage set to give gain $= 10^7$. Data for R7801 taken from [20], data for R11780 taken from [18].

5.2   Simulation parameters

The simulations incorporate the differing transit time distributions and PMT dimensions. The transit time distribution is approximated in the simulation by a composite distribution incorporating Gaussian distributions for the prompt and late pulsing (which is due to elastic scattering off the first dynode) and an exponential function for second pulsing (which is due to inelastic scattering off the first dynode). The charge distribution is approximated using a normalised gamma distribution with the parameters given in [18].

Simulations were run with a 20m right-cylindrical tank with a 1.6m/3.1m veto (which incorporates the 0.6m PMT support structure) between the tank wall and the PMTs in a 25m cylindrical cavern, surrounded by a 0.5m concrete layer on the walls and base and a 1m rock layer all the way around the cavern.

The number of 12" R11780 PMTs required to achieve the same coverage is significantly lower than the number of 10" R7801 PMTs required. The cost of the 12" SG PMT has been suggested to be less than 1.5 times the cost of the 10" SG PMT [16]. Total masses for the same coverage are comparable and as such the total radioactivity levels for the SG PMTs are also comparable.

5.3   Results

Event detection depends on the accuracy with which events can be reconstructed and this in turn is indicated by the vertex resolution. The vertex resolution is defined as the distance $\sigma = |\mathbf{x}_{reco} - \mathbf{x}_{true}|$ at which 68.2% of reconstructed events reconstruct within a sphere of radius r $= \sigma$ from the true vertex, i.e. the standard deviation of the reconstructed vertex from the true vertex.

Figure 2 shows a comparison between the vertex resolution of the two PMTs for positron (a) and neutron (b) events, plotted as a function of the light from the event, which is analagous to the energy of the charged particle. The vertex resolution can be described by the relation:

$$\sigma_{|\mathbf{x}_{reco} - \mathbf{x}_{true}|} = \frac{p0}{n9} + \frac{p1}{\sqrt{n9}} + p2 \tag{1}$$

where n9 is analogous to the energy and p0, p1 and p2 are shown on the plots [21]. The 12" PMT performs better on vertex reconstruction over the energy range of the signal, particularly for the lower-energy positrons.
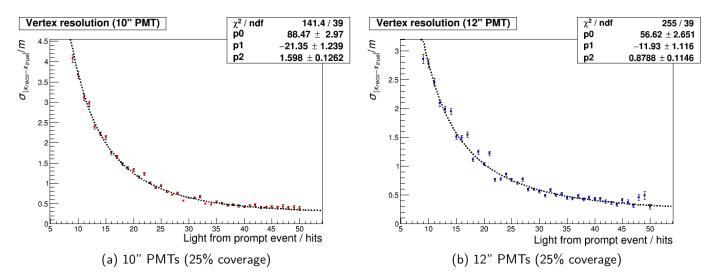
Figure 2: Comparison of vertex resolution for positrons of 10" and 12" PMTs, where 68% of vertices reconstruct within a sphere of radius σ from the true vertex.

Optimisation of the signal-to-background ratio is achieved by finding the optimal fiducialisation and energy cut. Fiducialisation - introducing a buffer volume between the PMTs and the fiducial volume from which we select our events - reduces the number of PMT background events in our selection but at some point we begin also to lose too many signal events. A cut on the minimum energy from an event cuts out the lowest-energy background events but if this minimum energy is set too high, signal events are also lost. So optimisation is a trade-off between maximising signal and minimising backgrounds. Figure 3 shows the method for assessing the maximal detector sensitivity for 10" (a) and 12" (b) PMTs, which gives a range where the signal-to-background ratio is maximised.

For the same coverage with a 1.6m veto and PMTs at 8.4m, the 10" SG and 12" SG PMTs have approximately the same radioactivity level and the optimal signal to background ratio is ~ 1.1 (~ 0.8) for the 12" (10") SG PMTs (figure 3).

(a) Signal to PMT background for 25% coverage with 10" SG PMTs

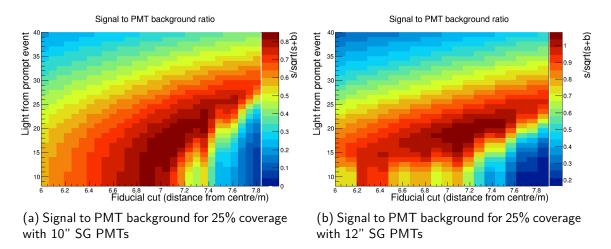(b) Signal to PMT background for 25% coverage with 12" SG PMTs

Figure 3: Preliminary comparison of signal to background for 25% with coverage 10" SG to 12" SG PMTs
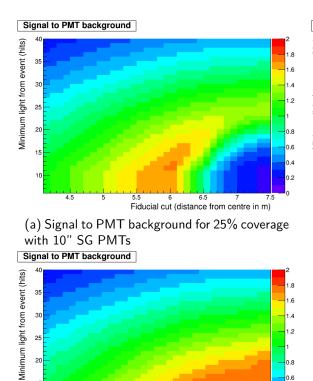
Dark noise in the PMT affects detection and reconstruction particularly at low energies. The dark rate for the same coverage is lower for the 12" PMTs due to the lower number of PMTs required to achieve the same coverage. The difference in the vertex resolution decreases with dark rate and this is seen in an increase in the number of interactions which reconstruct with sufficient accuracy (the 'trigger efficiency') in a detector instrumented with the 10" PMTs (table 3).

PMT	Trigger efficiency 10kHz dark rate	Trigger efficiency 8khz dark rate	Trigger efficiency 1kHz dark rate
10"	50.9	53.1	53.9
12"	53.9	53.9	53.9

Table 3: Dark rate-dependence of trigger efficiencies for positrons for 25% coverage of each PMT type, with minimum cut on light from event n9 = 9 hits.

The signal to PMT background ratio with a 3.1m veto and 6.9m-radius fiducial volume is higher for all PMTs. For the same coverage, the 10" SG and 12" SG PMTs again have approximately the same radioactivity level but preliminary results suggest that the optimal signal to background ratio of the 10" SG PMT is higher (~ 1.7) than that of the 12" SG PMT (~ 1.6). The signal to PMT background ratio with the 10" LRI PMT remains substantially higher at ~ 1.9.

The vertex resolution achieved for the smaller fiducial volume (of radius 6.9m) is better for both PMT sizes but in contrast to the results for the larger fiducial volume, the vertex resolution of the 10" PMT is comparable with, and in fact slightly better than, that of the 12" PMT. This suggests that the larger surface area of the PMT may be beneficial for vertex reconstruction over larger distances but that over shorter distances, less uncertainty on the position of the photon incident on the photocathode provided by using a smaller PMT may lead to better reconstruction.
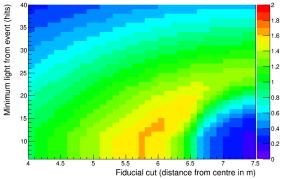
10

(a) Signal to PMT background for 25% coverage with 10" SG PMTs

(b) Signal to PMT background for 25% coverage with 12" SG PMTs

(c) Signal to PMT background for 25% coverage with 10" LRI PMTs

Figure 4: Preliminary comparison of signal to background with 25% coverage with 10" and 12" SG PMTs and 10" LRI PMTs

The ultimate aim of detector optimisation is to minimise the length of time to detection of a reactor. The example in figure 5 shows the number of experiment days required for detection of 1 core of the Hartlepool reactor to varying degrees of confidence, using a 20m tank with 10" LRI PMTs.
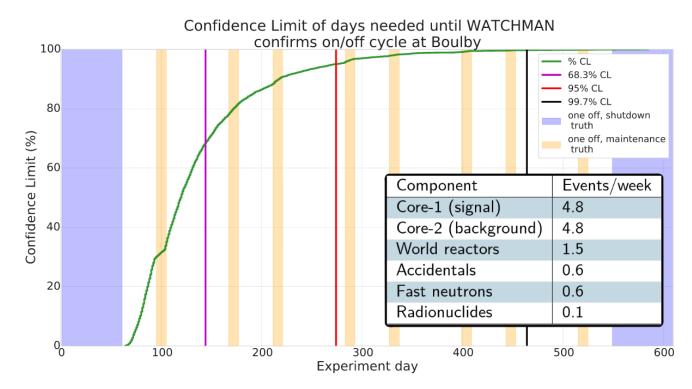

Figure 5: Confidence limit on the number of days required to confirm detection of the on/off cycle of a single core of the Hartlepool reactor with 25% coverage with $10''$ LRI PMTs. The red vertical line shows the number of days required to reach 95% confidence in the detection of one core of the Hartlepool reactor. The wide blue band signifies a long-duration core shutdown for maintenance and the narrower orange bands signify a shorter shutdown. [22]

5.4 Conclusions

An analytical method for optimising the signal-to-background ratio has been developed for the backgrounds due to PMT radioactivity in order to assess the effect of PMT radioactivity and PMT construction on the detector sensitivity. The method can be extended to include backgrounds from all sources for full detector optimisation.

It may be possible to achieve comparable sensitivity with standard-glass PMTs by increasing the distance between the PMTs and the fiducial volume and increasing the percentage of the inner volume surface area which is covered with PMTs. Since the cost of SG is lower than that of LRI glass and the cost of the 12" SG PMT has been suggested to be less than 1.5 times the cost of the 10" SG PMT, the results for the 10" and 12" SG PMTs could be further improved by using up to 30% coverage of the inner volume with PMTs.

The results for the 12" SG PMTs with a larger fiducial volume are particularly favourable. However, this assumes that the dark rate due to thermal emission of electrons from the photocathode is 10kHz per PMT. This has not yet been measured in water for these PMTs. With a lower dark rate, the sensitivity of the 10" PMTs is improved and it becomes harder to achieve comparable sensitivity with the 12" PMTs.

The signal-to-background ratio from 12" PMTs appears to be more sensitively dependent on the fiducial volume. For this reason, further assessment of the detector sensitivity with the 12" PMT requires careful optimisation of the location of the PMTs between tank wall and fiducial volume.

PMTs may be subject to implosion in the detector due to water pressure. Neither the 10" LRI PMT nor the 12" SG PMT has been pressure tested and there are concerns over the strength of both the low radioactivity glass and the larger-sized tube. The 10" SG PMT has passed stringent pressure testing [23] so in the event that the other PMTs were to fail pressure testing, up to 30% coverage with 10" SG PMTs could be considered.

6 Acknowledgements

References

[1] NNSA. Strategic Plan - Making the world a safer place. Technical report, NNSA, 2011.

[2] C. Palomares. Double-Chooz Neutrino Experiment, nov 2009.

[3] PROSPECT Collaboration, J. Ashenfelter, A. B. Balantekin, et al. The PROSPECT Reactor Antineutrino Experiment. jul 2018.

[4] I. Alekseev, V. Belov, V. Brudanin, et al. DANSS: Detector of the reactor AntiNeutrino based on Solid Scintillator. jun 2016.

[5] M Askins, M Bergevin, A Bernstein, et al. The Physics and Nuclear Nonproliferation Goals of WATCHMAN: A WAter CHerenkov Monitor for ANtineutrinos. 2015.

[6] D. Hellfeld, A. Bernstein, S. Dazeley, and C. Marianno. Reconstructing the direction of reactor antineutrinos via electron scattering in Gd-doped water Cherenkov detectors. *Nuclear Instruments and Methods in Physics Research, Section A: Accelerators, Spectrometers, Detectors and Associated Equipment*, 841(October 2016):130–138, 2017.

[7] N. S. Bowden, A. Bernstein, S. Dazeley, et al. Observation of the isotopic evolution of pressurized water reactor fuel using an antineutrino detector. *Journal of Applied Physics*, 105(6), 2009.

[8] K Scholberg. Supernova neutrino detection. *Annual Review of Nuclear and Particle Science*, 62:81–103, 2012.

[9] P. Vogel and J. F. Beacom. Angular distribution of neutron inverse beta decay. *Physical Review D*, 60(5):10, 1999.

[10] Adam Bernstein, Todd West, and Vipin Gupta. An assessment of antineutrino detection as a tool for monitoring nuclear explosions. *Science & Global Security*, 9(3):235–255, jan 2001.

[11] John F. Beacom and Mark R. Vagins. GADZOOKS! Antineutrino Spectroscopy with Large Water Cerenkov Detectors. pages 1–4, 2003.

[12] M Ikeda. GADZOOKS! project at Super-Kamiokande. In *WIN2015*, 2015.

[13] M. Yeh, S. Hans, W. Beriguete, et al. A new water-based liquid scintillator and potential applications. *Nuclear Instruments and Methods in Physics Research Section A: Accelerators, Spectrometers, Detectors and Associated Equipment*, 660(1):51–56, dec 2011.

[14] B W Adams, K Attenkofer, M Bogdan, et al. A Brief Technical History of the Large-Area Picosecond Photodetector (LAPPD) Collaboration. 2016.

[15] H. Löhner, Q Dorosti-Hasankiadeh, E Heine, et al. The multi-PMT optical module for KM3NeT. *Nuclear Instruments and Methods in Physics Research, Section A: Accelerators, Spectrometers, Detectors and Associated Equipment*, 718:513–515, 2013.

[16] Sean Grullon. Characterization of the Hamamatsu R11780 12-inch Photomultiplier tube Neutrino Mixing Angles Measured with Optical Detectors Super-K Daya Bay.

[17] A. G. Wright. *The Photomultiplier Handbook*. 2017.

[18] J. Brack, B. Delgado, J. Dhooghe, et al. Characterization of the Hamamatsu R11780 12 in. photomultiplier tube. *Nuclear Instruments and Methods in Physics Research, Section A: Accelerators, Spectrometers, Detectors and Associated Equipment*, 712:162–173, 2013.

[19] Hamamatsu Photonics. LARGE PHOTOCATHODE AREA PHOTOMULTIPLIER TUBES, 2012.

[20] Hamamatsu Photonics. Photomultiplier Tubes. *Experimental Methods in the Physical Sciences*, 2013.

[21] M Bergevin. Results of the WATCHMAN Detector Monte Carlo. pages 1–10, 2013.

[22] Teal Pershing. AIT-WATCHMAN/WATCHStat: Python software for analyzing expected IBD signal rates in WATCHMAN. 2018.

[23] K. Chambliss, S.K. Sundaram, N. Simos, and M.V. Diwan. Photomultiplier tube failure under hydrostatic pressure in future neutrino detectors. *Journal of Instrumentation*, 9(10):T10002–T10002, 2014.